Frequency Response of Aerodynamic Load Control through Mini-tabs

D. J. Heathcote[1], I. Gursul[2], D. J. Cleaver[3]
Department of Mechanical Engineering, University of Bath, BA2 7AY, UK

Load control is the reduction of extreme aerodynamic forces to enable lighter, more efficient aircraft. Current load control technologies are limited to low frequency disturbances. In this paper the mini-tab, a small, span-wise tab placed on the airfoil upper surface, is investigated as a high frequency alternative through periodic oscillations to identify its unsteady aerodynamic transfer function. Force measurements were conducted on a NACA0012 airfoil at a Reynolds number of 6.6×10^5 with a deployable mini-tab located at $x_f/c = 0.85$, with actuation performed at reduced frequencies, $k \leq 0.79$. The force measurements indicate that the mini-tab has a decreasing effect on lift reduction with increasing actuation frequency. This trend is comparable to Theodorsen's function, based on the change in circulation. For $\alpha = 0°$, the normalized peak-to-peak lift reduction decreased from 1 for steady state deployment to around 0.6 at $k = 0.79$. In addition, a phase lag exists between the mini-tab deployment and the aerodynamic response which increased with actuation reduced frequency, k. However, the measured phase lag is substantially larger than Theodorsen's prediction. Increasing the angle of attack, α reduced the mini-tab's effect on lift while increasing the phase angle when comparing equal k values. Particle Image Velocimetry measurements indicate that the delay and reduction in effectiveness of periodic deployment is due to the presence and growth of the separated region behind the mini-tab. Overall, the mini-tab was found to be an effective, dynamic lift reduction device with the separated region behind the mini-tab key to the amplitude and phase delay of lift response.

Nomenclature

α	=	angle of attack
b	=	span
c	=	airfoil chord length
$C(k)$	=	Theodorsen's circulation function
C_L	=	time-averaged lift coefficient, $L/0.5\rho U_\infty^2 bc$
$C_{L,\,h=0}$	=	time-averaged lift coefficient for $h = 0$
$C_{L,\,hmax}$	=	time-averaged lift coefficient for h_{max}
$C_{L,\,max}$	=	maximum phase-averaged lift coefficient
$C_{L,\,min}$	=	minimum phase-averaged lift coefficient
$\Delta C_{L,ss}$	=	change in lift coefficient from baseline configuration, steady state, $C_{L,\,hmax} - C_{L,\,h=0}$
$\Delta C_L(t)$	=	change in lift coefficient from baseline configuration, time dependent, $C_L(t) - C_{L,\,h=0}$
$\Delta C_{L,mean}$	=	mean phase averaged change in lift, $C_{L,mean} - C_{L,\,h=0}$
f	=	frequency of actuation
h	=	mini-tab height
h_{max}	=	maximum mini-tab height
k	=	reduced frequency of actuation, $\pi f c/U_\infty$
q	=	free-stream dynamic pressure, $0.5\rho U_\infty^2$
Re	=	Reynolds number, $\rho U_\infty c/\mu$
t	=	time
T	=	Period of mini-tab deployment

[1] Postgraduate Student, Department of Mechanical Engineering. Student Member AIAA.
[2] Professor, Department of Mechanical Engineering. Associate Fellow AIAA.
[3] Lecturer, Department of Mechanical Engineering. Member AIAA.

U_∞ = free-stream velocity
p_∞ = free-stream static pressure
ρ = fluid density
u = velocity component parallel to free-stream
v = velocity component perpendicular to free-stream
μ = dynamic viscosity
x = chord-wise location
x_f = mini-tab chord-wise location
y = position perpendicular to free-stream
z = span-wise location

I. Introduction

The subject of aerodynamic flow control through both active and passive means has become an increasingly important topic in recent years. In order to simultaneously meet environmental demands, i.e. the ACARE Vision 2020 and Flightpath 2050 legislation and increased demand from passengers, innovative solutions across all areas of the aircraft must be examined to solve the nascent problems within modern aviation.

The aircraft wing box, located between the wings, is one of the largest and heaviest structures on the aircraft. Its strength and stiffness is defined by the most extreme loads, those generated during gusts, turbulence and extreme maneuvers, even though these events rarely occur. These events are typically short but severe in nature, with a maximum reduced frequency, k up to 1 possible[1]. Current load alleviation strategies use large control surfaces such as the aileron or spoiler, however, these devices are large and have a poor frequency response. As such, managing the higher frequency loads passed to the airframe remains an important issue facing the aircraft designer. Therefore, an innovative and effective loads mitigation technique that is effective across the entire frequency range is needed.

A wide variety of novel flow control strategies have been proposed and examined, through both fluidic and mechanical means[2-4], to reduce lift and manage aerodynamic loads. Research into two of these devices, the jet-flap and mini-tab, has been conducted at the University of Bath[5,6]. This research has shown both actuators to be effective lift control strategies in a static configuration (i.e. steady blowing or a stationary mini-tab). The focus of this study is to investigate the effectiveness of the mini-tab during dynamic, periodic deployment.

The mini-tab consists of a small, span-wise tab placed normal to the surface of the airfoil. This type of device is used widely in the form of the Gurney flap for lift increase through application close to the trailing edge on the lower surface. As first hypothesized by Liebeck[7], a counter-rotating vortex pair is initiated behind the tab, creating a change in the circulation about the airfoil. The separated region creates effective increase in the airfoil camber, with a displacement in the Kutta condition downstream of the airfoil trailing edge. This moves the final part of the pressure recovery off-surface, increasing overall suction. Upper surface placement produces the reverse effect: a lift decrease with previous work[5] finding similar effects to those hypothesized by Liebeck at zero angle of incidence. The theory of Liu & Montefort[8] suggests that mini-tab lift reduction scales with the square root of mini-tab height.

Figure 1 illustrates the previously evaluated[5] lift coefficient and flow-field measurements at a range of chord-wise locations, x_f/c and angles of attack, α. The mini-tab's effect on lift was determined to be highly dependent on both parameters. For a normalized height, h/c = 0.02, mini-tab placement close to the trailing edge had a decreasing effect with increasing angle of attack towards stall, as the baseline flow separation engulfs the mini-tab. Utilization close to the mid-chord (x_f/c = 0.60) produces a large lift reduction across a wide range of angles of attack (α = 0 to 5°) with a steady state change in lift coefficient, $\Delta C_{L,ss}$ of up to -0.60 for a mini-tab of height, h/c = 0.04. As with the trailing edge location, the mid-chord reduces in effectiveness towards stall. Placement close to the leading edge (x_f/c = 0.08) efficiently separated the flow at low incidences with little change in lift due to flow reattachment, however, with increasing angle of attack a corresponding increase in lift reduction can be observed with $\Delta C_{L,ss} \approx$ -0.68 feasible for h/c = 0.04.

Although the mini-tab has been found to be effective at reducing lift in steady-state or static deployment, the dynamic effects of deployable mini-tabs have been less widely evaluated. Investigation of these effects is key to determining its usefulness as a high frequency actuator, in terms of any phase delay between deployment and aerodynamic effect and amplitude of lift change with respect to deployment frequency, k. From this, an aerodynamic transfer function could be determined, allowing for the design of an accurate and robust controller for aerodynamic loads control during gusts.

The majority of previous research has been completed at reduced frequencies that are lower than those required for the current application, with $k < 0.2$ typical for most experimental measurements[9]. This reduced frequency is indicative of actuation on a helicopter blade, where lift augmentation on the retreating blade is desired and is a function

of the blade frequency. Matalanis et al[10] investigated a mini-tab like device oscillating at reduced frequencies between $k = 0.032$ and 0.16. The results of this study indicated that the mini-tab's ability to augment lift reduced with increasing deployment frequency along with an associated delay in response. The study of Tang & Dowell[11] indicated the opposite trend, with an increase in actuation frequency producing an enhancement in aerodynamic loading, also noting the delay in aerodynamic response. The computations of Kinzel et al[12] provide the largest ranging study in the effects of mini-tab use at higher reduced frequencies. The effects are evaluated computationally for a range of airfoil profiles and test conditions with reduced frequencies, $k \leq 1$. Expressed in terms of a normalized lift augmentation ratio, results show a reasonable agreement with the trends predicted by Theodorsen's circulation function[13], which has been widely used in the field of oscillating airfoils. This is corroborated by the work of Lee & Kroo[14], who found similar trends in amplitude. Phase angle between mini-tab deployment and lift augmentation was found to increase with reduced frequency in line with Theodorsen's function[12,14]. However, the function has some limitations in its derivation: any non-linearities in the flow-field such as vortex interaction are not considered. The flow behind the mini-tab is highly separated and thus experimentation is key to fully evaluating the actuator's effects and predicting the non-linear behavior. Additionally, it has been noted that as the deployment reduced frequency increases, a hysteresis loop[10,11] develops, when the time dependent change in lift, $\Delta C_L(t)$ is compared to the normalized mini-tab deployment, h/c. Kinzel et al[12] also note the effect of upstream mini-tab employment, suggesting that the hysteresis loop develops more quickly for upstream placement than for placement at the trailing edge with respect to the deployment reduced frequency, k.

This paper presents experimental measurements for a sinusoidally oscillating mini-tab at reduced frequencies of up to $k = 0.79$. The experiments investigate the effect on lift reduction and phase angle between mini-tab deployment and lift response across a wide range of angles of incidence with the mini-tab placed close to the trailing edge. In addition, phase-locked Particle Image Velocimetry measurements are displayed to indicate the effects of the mini-tab on the flow in the vicinity of the airfoil. The current study aims to investigate the mini-tab at higher than previously measured reduced frequencies to determine the mini-tab's aerodynamic properties.

II. Experimental Apparatus and Procedure

A. Experimental Setup

The experiments presented were all completed at the University of Bath's large wind tunnel facility. The test section has dimensions of 2.13 x 1.51 x 2.70 m and uses an octagonal cross-section to reduce the influence of secondary flow effects. The wind tunnel itself is of a closed loop design. The free-stream velocity, U_∞ used during the experiments was 20 ms^{-1} with a turbulent intensity of less than 0.5%. Figure 2 illustrates the working section, with the wing *in-situ* and air bearing force balance set up shown above the wind tunnel.

Figure 3 shows a schematic of the wing used for the tests. A NACA0012 profile was utilized due to its symmetric nature and the wide range of data available in the literature. A Reynolds number, Re of 6.6×10^5 was obtained based on the airfoil chord, $c = 0.5$ m. The span, b was chosen to be 1.5 m such that the wing fully traversed the cross-section of the tunnel with a small clearance of 5 mm or 0.3% of the overall span. This avoided physical interference with the wind tunnel walls to provide accurate measurements, while creating test conditions analogous to that for an infinite span via the use of the wind tunnel walls as end plates. Boundary layer transition was promoted via the use of a trip wire at the point of maximum velocity, as suggested by Barlow[15]. Using the methods described by Pankhurst & Holder[16], a wire of diameter 0.3 mm was placed at a chord-wise location of $x/c = 0.10$.

The wing itself is constructed in two parts as shown in Fig. 3(a). The initial $0.725c$ is constructed from a carbon fiber composite with an aluminum support structure comprising endplates and a mounting spigot to create a rigid yet light wing. The final $0.275c$ of the profile is constructed from selective laser sintered (SLS) Nylon and was made in five 0.3 m sections. This allowed for alteration of the actuation method (mini-tab or jet flap) in the vicinity of the trailing edge.

The mini-tab's chord-wise location was $x_f/c = 0.85$ with a maximum mini-tab height, $h_{max}/c = 0.015$ achievable. The location was chosen as the closest point to the trailing edge where the deployment height could be produced due to the geometric constraints of the trailing edge. Previous measurements[5] have shown that the static lift reduction of $x_f/c = 0.85$ is extremely similar to that for locations closer to the trailing edge, *i.e.* $x_f/c = 0.95$. The mini-tab itself was constructed from 3 mm thick acrylic and is of length 1475 mm, providing a small gap at either end equal to 0.8% of the overall span, b to avoid interference with the wind tunnel walls. Due to the size constraints of the trailing edge section the ideal, linear deployment profile for the mini-tab was not achievable. Instead the mini-tab uses two rotational elements per section supported on a pair of micro ball-bearings, with the mini-tab moving through a slight arc as shown in Fig. 3(b). A difference in mini-tab angle of 13° between the minimum and maximum deployment heights is

created by the setup. Measurements by Wang et al[17] indicate that, for angles close to normal to the surface, the effect of mini-tab angle on lift augmentation was negligible.

The actuation mechanism for the mini-tab is shown in Fig. 3(c). Actuation of the mini-tab is provided by an array of five Voice Coil Actuators (VCAs), one per trailing edge section. The BEI-Kimco LA08-10-000A VCA was positioned in a chord-wise direction, with the linear motion of the VCA translated through 90° by a linkage. The VCAs provided a displacement amplitude of 4 mm, which was increased by the linkage to a maximum mini-tab deployment of 7.5 mm corresponding to $h_{max}/c = 0.015$. The design is similar to that evaluated by Tsai et al[18], however the linkage is of a sliding design, opposed to the pinned, 4 bar linkage mechanism used in the literature.

In order to accurately monitor and produce the desire actuation profile, the mini-tab's motion was controlled using a PID controller: the GALIL DMC-30012. The deployment of the mini-tab is monitored by a Renishaw RGH-34 encoder with a resolution of 0.01 mm. This provides displacement feedback to the controller which, through a PID control algorithm with additional feedforward velocity and acceleration terms, allowed the desired deployment profile, generated by a National Instruments compact RIO (cRIO), to be accurately executed. In the measurements presented within this paper, displacements of h_{max}/c = 0.01 and 0.015 were accurately achieved up to deployment reduced frequencies, k of 0.79 with maximum average deployment error of less than 5%.

B. Force Measurements

The airfoil was mounted in the test section from above via a new innovative design of force balance. Frictionless air bearings support the weight of the wing and force balance carriage and are aligned in a direction parallel to that of the lift force produced by the airfoil (y-axis). The air bearings remove any bending moment to leave pure lift force allowing for a sensitive force measurement apparatus with high frequency response. The load was applied through a FUTEK S-type strain gauge based force transducer.

The signal from the force transducer was conditioned and acquired using a National Instruments cRIO system. In addition, the cRIO provides and monitors the actuator's input and acquires mini-tab's position. By acquiring all 3 concurrently, any delay in the response of the aerodynamic system or mechanical system could be accurately determined. The force and input signals were acquired at 5 kHz. The mini-tab's position was acquired in the form of a quadrature signal at 50 kHz; the high acquisition frequency was required due to the mini-tab's high peak velocity.

Before each set of experiments, a static calibration was performed in order to find a force-voltage constant via a linear regression. Forces in the form of known weights were applied such that the constant could be determined using a minimum of 10 discrete data points between 0 and 150 N.

In order to facilitate accurate measurement of the angle of attack, α, the air bearing carriage includes an integrated SICK rotary encoder with a measurement accuracy of ± 0.02°. Angles of attack, α = 0, 5, 8, 10 and 13° were used to investigate the effects of dynamic mini-tab actuation at angles of attack up to and including stall. Table 1 summarizes the experimental parameters investigated during the force measurements.

Table 1: Table displaying experimental parameters, associated values and experimental uncertainty.

Parameter	Range or Value Considered	Uncertainty
***h/c*, mini-tab height**	0.01 to 0.015	±0.0005
***x_f/c*, chord-wise position**	0.85	±0.003
***Re*, Reynolds number**	6.61×10^5	$\pm 0.16 \times 10^5$
***α*, Angle of Attack**	0, 5, 8, 10 & 13°	±0.25°
***k*, actuation reduced frequency**	0 to 0.79	±1.8 % k

C. Dynamic Force Balance Calibration

A dynamic force balance calibration was completed, using the comparison method as outlined by Kumme[19], before aerodynamic force measurements were performed. This calibration experiment, completed in quiescent air, allows a transfer function between the measured force by the force balance and a known input force to be determined. This allows for any system resonant modes to be accounted and corrected for. During this calibration, an electro-mechanical shaker was placed outside the wind tunnel and connected to the wing at its center of mass. The shaker creates a sinusoidal load which is passed through an in-line FUTEK force transducer to the wing. By monitoring the two force transducer signals a transfer function, in terms of phase delay and amplitude ratio between the air bearing force balance and the known input and measured output force, can be determined. The experiment was performed over 100

sinusoidal cycles of oscillation between 0 and 20 Hz at a frequency resolution of 0.5 Hz, with a phase averaged solution used in order to calculate the values relevant to the transfer function. The uncertainties in the calibration were quantified using the methods of Moffat[20], with a typical uncertainty in amplitude ratio of ±2% (5% at resonance) and in phase angle of ±0.25° (±5° at resonance) calculated.

The results of the dynamic force balance calibration are shown in Fig. 4. From the measurements it can be noted that the first natural frequency of the system exists at around 7.25 Hz. At this frequency the amplitude ratio between input force and the force measured by the force balance peaks at around 20. In terms of phase angle, a rapid change exists at around 7.5 Hz, once again indicating resonance. It was determined that the amplitude ratio at 7.25 Hz is too high to reliably and accurately measure the aerodynamic forces during experiments. As such, no measurements will be reported between 7 and 7.5 Hz, corresponding to reduced frequencies of $k = 0.55$ and 0.59. A second smaller resonant mode exists at around 13 Hz, indicated by a peak in phase angle and a plateauing in the amplitude ratio. The input force to the force balance-wing system was varied between ±10, 25 and 50N. It can be seen that there is a very good agreement between the different input force values, indicating that there is no effect of input force on the dynamic response.

D. Measurement Processing

After acquisition all measurements were processed using MATLAB. In order to calculate both the amplitude and phase angle information required for the calibration experiment and the dynamic force measurements, a frequency domain processing method was employed. The raw data was converted using a Fast Fourier Transform, from which the amplitude and phase could be easily extracted for both mini-tab input and lift response. During the dynamic force measurements, the dynamic calibration transfer function was applied as a correction in the frequency domain. The measurements were then converted back to the time domain. As with the calibration experiment, the measurements were phase-averaged with a minimum of 100 phases considered.

E. Particle Image Velocimetry Measurements

Cases of interest were selected for further analysis using Particle Image Velocimetry (PIV). A TSI 2D-PIV system was used for the measurements. This consisted of a double pulsed 200 mJ 15 Hz Nd:YAG Quantel Evergreen laser, two eight Megapixel TSI PowerView CCD cameras (3,312 x 2,488 pixels) using Nikon 50 mm Nikkor lenses, a TSI LaserPulse synchronizer and a six jet TSI oil-droplet generator. The two cameras were mounted on a traverse below the wind tunnel in a "tandem" configuration. The cameras employ the same plane of interest, located at a span-wise location of $z/b = 0.6$ and are positioned 1 m below the wind tunnel. This span-wise location avoids disturbance of the flow due to the presence of pressure tappings at the mid-chord. The measurement plane was orientated normal to the airfoil chord. The dual camera setup allowed the full airfoil upper surface and wake to be viewed, with an overall field of view of 0.8 x 0.3 m. In this paper, a region of interest was selected close to the airfoil trailing edge in order to better show the subtle differences between the cases.

For each case a series of 500 image pairs were concurrently acquired for each camera. For the phase-locked measurements a synchronization pulse was used between the National Instruments cRIO system and the TSI synchronizer. The pulse could be accurately positioned within the mini-tab's desired profile at normalized phase values of $t/T = 0.0, 0.25, 0.5, 0.75$ in order to fully analyze the effects of the deploying mini-tab at those four positions in its deployment cycle.

TSI Insight 4G software was used to determine the in-plane velocity vectors using a fast Fourier transform cross-correlation algorithm between the image pairs. An interrogation region of 32 x 32 pixels was chosen, producing a spatial resolution of 0.2*%c*. In addition, an overlap between the cameras was used such that the two vector fields, one produced by each camera, could be accurately merged using MATLAB. A weighted average was used within the overlap region with a bias towards the closer image center.

III. Results and Discussion

Shown in Fig. 5 is the nomenclature that will be used throughout this section to represent the steady-state and periodic lift coefficients. Firstly, the steady-state change in lift, $\Delta C_{L,ss}$ is defined as the difference between the time averaged lift coefficient for the clean airfoil where no mini-tab is used, $C_{L,h=0}$ and the time-averaged lift coefficient corresponding to the maximum mini-tab height, $C_{L,hmax}$. The maximum mini-tab height corresponds to the maximum value used in the periodic measurements: either $h_{max}/c = 0.01$ or 0.015. When oscillated periodically the mini-tab will produce a lift coefficient that is likewise periodic, $C_L(t)$. The periodic and time dependent change in lift, $\Delta C_L(t)$ is defined as $C_L(t) - C_{L,h=0}$. This periodic lift coefficient will have a phase-averaged maximum, $C_{L,max}$ and minimum, $C_{L,min}$. Therefore, $C_{L,min} - C_{L,max}$ refers to the phase-averaged peak-to-peak change in lift for a particular reduced frequency. Finally, the mean change in lift, $\Delta C_{L,mean}$ is once again measured from the baseline, clean configuration, $C_{L,h=0}$.

A. Baseline Steady-State Measurements

Figure 6 shows steady-state lift measurements for angles of attack, α between 0° and 13°. The mini-tab was held at a static position between heights, h/c between 0 and 0.015. Lui & Montefort[8] theorized that the mini-tab should produce a steady-state change in lift proportional to the square root of the normalized mini-tab height:

$$\Delta C_{L,ss} \propto \left(\frac{h}{c}\right)^{\frac{1}{2}}$$

Previous measurements[5] along with comparison to existing literature[21,22] for mini-tab locations close to the trailing edge have indicated that this expression, based upon thin airfoil theory, is valid for a range of airfoil profiles at zero degrees incidence[5]. In comparison to the theory, Fig. 6 indicates that for the present chord-wise location, $x_f/c = 0.85$, there is reduction in effectiveness at small mini-tab deflections. This indicates that the square-root relationship is invalidated for this configuration. The small $\Delta C_{L,ss}$ values may be due that at small mini-tab heights, the mini-tab has a lower effectiveness than at larger displacements, with the reduction in velocity close to the surface within the boundary layer inhibiting the mini-tab's ability to reduce lift. As such, to better fit the behavior of the mini-tab at all angles of attack a cubic regression is applied as a line of best fit, rather than the square-root relationship. This better represents the relationship and will be used as quasi-steady response ($k \rightarrow 0$) in Section III.B. The steady-state response, $\Delta C_{L,ss}$ is used to normalize the dynamic lift change measurements, allowing for accurate comparison of the mini-tab's effect between angles of attack.

As α increases towards stall at 13°, the steady-state change in lift decreases in line with previous measurements. A reduction in $\Delta C_{L,ss}$ from -0.17 at zero degrees to -0.04 at 13° is observed for a mini-tab height of $h/c = 0.015$. The reduction, as previously stated, can be attributed to the movement of flow separation to ahead of the mini-tab location at high angles of attack, inhibiting the mini-tab's influence on the flow.

B. Periodic Force Measurements

Dynamic mini-tab measurements were completed at angles of attack from 0° to stall at $\alpha = 13°$, to fully evaluate effect of reduced frequency. The results are presented in Figs. 7 to 11 for mini-tab deployment up to $h_{max}/c = 0.01$ and 0.015.

Firstly, Fig. 7 presents the phase-averaged, time dependent change in lift, $\Delta C_L(t)$, normalized by the steady-state value, $\Delta C_{L,ss}$. This is presented for three reduced frequencies, $k = 0.2$, 0.39 and 0.63 for a maximum mini-tab deployment of $h_{max}/c = 0.015$ and angle of attack, $\alpha = 0°$. This is presented as a function of the normalized time within the phase, t/T where T is the period of oscillation. A t/T value of 0 indicates that the mini-tab is fully stowed within the airfoil surface, whereas $t/T = 0.25$ & 0.75 represent a mini-tab which is half deployed ($h/c = 0.0075$) and $t/T = 0.50$ is the fully deployed ($h/c = 0.015$) condition. In addition, a $k \rightarrow 0$ indicates the steady-state value. This is equivalent to a case where the mini-tab is moved infinitely slowly such that steady-state aerodynamics are conserved. By definition for this case, a maximum value $\Delta C_L(t)/\Delta C_{L,ss} = 1$ is obtained at $t/T = 0.5$. In addition, it can also be noted that the response is not a perfect sine wave. This is due to the non-linearity in $\Delta C_{L,ss}$ with respect to the mini-tab height, h/c.

In comparison to steady-state deployment, actuation of the mini-tab at a reduced frequency, $k = 0.2$ indicates a decrease in the lift reducing ability of the mini-tab, reaching a peak normalized value of $\Delta C_L(t)/\Delta C_{L,ss} = 0.93$. The phase-averaged results are shifted to the right when compared to the $k \rightarrow 0$ case, implying a delay between the deployment of the mini-tab and the corresponding aerodynamic response.

Increasing the actuation frequency further to k = 0.39 and 0.63 indicates the same trend, with a decrease in the amplitude of the phase-averaged measurements with an increased phase delay. Additionally, clear non-linearities in the aerodynamic response can be noted, most clearly for k = 0.63 where a double peak in $\Delta C_L(t)/\Delta C_{L,ss}$ is observed.

In order to investigate the effects of increased reduced frequency, a wide range of measurements were conducted between k = 0.04 and 0.79, with values close to the system resonant frequency (k = 0.55 and 0.59) omitted due to the relatively high uncertainty. These results are presented in Figs. 8 to 11. First, in Fig. 8 the measurements are presented in the form of the phase-averaged peak-to-peak change in lift, $C_{L,min} - C_{L,max}$ calculated as the difference between maximum and minimum lift coefficient within the phase averaged data (see Fig. 5).. By comparing Figs. 8(a) to (e) it can be noted that the $C_{L,min} - C_{L,max}$ at zero degrees is much larger than that for 13°, which is consistent with the steady-state measurements. For all angles of attack, it can be observed that as the reduced frequency of sinusoidal mini-tab actuation, k is increased the lift reducing ability of the mini-tab reduces.

In order to better consider the decay in the peak-to-peak change in lift, $C_{L,min} - C_{L,max}$ is normalized by the respective steady-state value, $\Delta C_{L,ss}$ and is presented in Fig. 9. Also included is Theodorsen's circulation function, $C(k)$. Figure 9(a) presents measurements taken at α = 0°. A decay in the normalized peak-to-peak change in lift, $(C_{L,min} - C_{L,max})/\Delta C_{L,ss}$ can be clearly observed, with Theodorsen's function showing a good agreement. This result is surprising, given the derivation of Theodorsen's function, which is intended for pitching and plunging airfoils without any consideration for flow separation as produced by the mini-tab.

Figures 9(b) to (e) indicate the effects of increasing the angle of attack, α on the normalized peak-to-peak change in lift. Increasing the angle of attack reduces the mini-tab's effectiveness as the reduced frequency, k is increased. This is most noticeable for stall, corresponding to an angle of attack of 13° (Fig. 9(e)), where a more rapid decrease in $(C_{L,min} - C_{L,max})/\Delta C_{L,ss}$ is observed than at α = 0°.

Figure 10 presents the phase angle of the phase-averaged signal. This was calculated from the first harmonic of the lift response, corresponding to the mini-tab actuation frequency. A more negative phase angle indicates a greater delay in lift response. The measurements for α = 0° indicate an almost monotonic increase in the phase angle, φ with respect to reduced frequency, k. When comparing h_{max}/c = 0.01 and 0.015 it is evident that there is an agreement between the two maximum mini-tab heights, suggesting that there is no effect of mini-tab height on phase angle. In addition, when compared to Theordorsen's function there is little agreement, with a much larger magnitude phase angle generated for the mini-tab measurements. Comparing Figs. 10(a) to (e) it can be noted that the phase angle increases as the angle of attack increases.

Finally, Fig. 11 presents the phase-averaged mean change in lift, $\Delta C_{L,mean}$.as a function of reduced frequency, k. For α = 0°, as with the previous static measurements, it can be noted that h_{max}/c = 0.015 produces a larger $\Delta C_{L,mean}$ than h_{max}/c = 0.01. As the frequency of actuation increases, it can be noted that there is not a significant alteration in $\Delta C_{L,mean}$. Figs. 11(b) to (e) also show that effect is consistent when the angle of attack is increased. In conjunction with the decrease in the peak-to-peak change in lift, the constant mean value indicates that the lift coefficient does not return to the steady-state minimum or maximum lift coefficient values for high frequency actuation, and rather reduces about a mean value.

Overall, the behavior of the mini-tab is similar to that evaluated computationally[12,14] in terms of lift augmentation ratio with a decrease comparable to Theodorsen's function but not in terms of phase angle. In addition, there still exists a need to evaluate the effect of periodic deployment on the flow-field in order to understand the mechanisms and large phase lags involved with periodic mini-tab deployment.

C. Phase-Locked Particle Image Velocimetry Measurements

Figures 12 and 13 present time-averaged and phase-locked velocity magnitude and vorticity at α = 0° for phase positions of t/T = 0.0, 0.25, 0.5 and 0.75. Additionally, the corresponding $\Delta C_L(t)/\Delta C_{L,ss}$ data is presented for comparison.

Firstly, the steady-state effect of mini-tab employment, corresponding to $k \rightarrow 0$ is considered in the first column in Figs. 12 and 13. The mini-tab positioned at t/T = 0.25 and 0.50 corresponds to a normalized mini-tab height, h/c = 0.0075 and 0.015, equating to 50% and 100% of the deployment range. In line with previous measurements, the increase in mini-tab height produces a larger recirculation region behind the mini-tab. The recirculation region is key to the mini-tab's effectiveness, causing an effective decrease in the airfoil camber reducing lift. Also, Fig. 13 shows that the region of vorticity present behind the mini-tab increases in size with increasing deployment height and is displaced further away from the surface. This indicates that the shear layer produced by the mini-tab is displaced further away from the surface. It is important to note that, for a steady-state measurement ($k \rightarrow 0$), t/T = 0.25 and 0.75 are the same by definition.

In order to analyze the effects of a periodically deploying mini-tab on the flow, each position in the phase will be analyzed individually. For t/T = 0.00 the mini-tab is fully stowed within the trailing edge. The phase-averaged force

measurements indicate an increasing delay in lift response as k is increased. Although the effect is subtle between the three reduced frequencies, by looking at the streamlines present in Fig. 12 it can be observed that increasing k from 0.20 to 0.63 causes a slight upward displacement in the streamlines, indicating a decrease in lift. This effect can more clearly be observed in Fig. 13, where the region of negative vorticity emanating from the upper surface is displaced further upwards for $k = 0.63$ than 0.20.

Moving to $t/T = 0.25$, the mini-tab is now positioned at $h/c = 0.0075$. The delay in lift is more clearly observable for this position. In Fig. 12 it is noticeable that as k increases the separated region behind the mini-tab decreases, indicative of a reduction in effect. This is also observable in Fig. 13, where a reduction in the size of the region of vorticity behind the mini-tab is present. This corroborates the results found during the force measurements, which indicate a reduction in mini-tab effect as k increases.

The delay and reduction in effectiveness is less clear at $t/T = 0.50$, where the separated region behind the mini-tab appears to be similar for the three reduced frequencies. This is despite the relatively large differences in phase-averaged lift coefficient present at this time. The clearest comparison is between $k \rightarrow 0$ and $k = 0.63$ where the separated region appears smaller for the periodically deployed mini-tab. Due to the sinusoidal deployment profile, the change in mini-tab height close to the maximum value is small with respect to time. In addition, the gradient of the steady-state change in lift, $\Delta C_{L,ss}$ gets smaller with respect to height close to $h_{max}/c = 0.015$. It may be that phase delay is masked by the relatively small changes in lift close to the maximum mini-tab height, thus producing a small difference in flow-field.

At $t/T = 0.75$ the effect of reduced frequency is once again easily observable. At this position, the mini-tab is retracting and thus a lag in response is indicated by an increase in the separation region's size. This is observable in Fig. 12, where moving from $k = 0.20$ to 0.63 produces a larger separated region and an increased effect on lift coefficient (a greater lift reduction when compared to $k \rightarrow 0$).

In summary, the PIV measurements clearly show the effects of a periodically deploying mini-tab on the flow-field. A separated region is initiated by the mini-tab which grows and shrinks throughout the deployment cycle. The separated region deflects the wake upwards, providing an effective reduction in the airfoil camber, reducing lift. The aerodynamic lag and alteration in effectiveness most clearly observable for $t/T = 0.25$ and 0.75 respectively and are in good agreement with the force measurements.

IV. Conclusions

A mini-tab located at $x_f/c = 0.85$ was actuated with a sinusoidal profile of amplitude, $h_{max}/c = 0.01$ and 0.015 at reduced frequencies, k up to 0.79. It was found that the mini-tab is an effective lift reduction device. As actuation reduced frequency is increased, it was found that the mini-tab's ability to reduce lift was inhibited, with a peak-to-peak lift reduction of 60% of the static value obtained for $k = 0.79$ and amplitude, $h_{max}/c = 0.01$. Additionally, it was found that for all angles below stall, the normalized lift reduction of the mini-tab compared favorably to Theodorsen's circulation function. However, the phase angle generated was not comparable, being much larger for mini-tab deployment. The angle of attack of the airfoil, α also produced a significant effect, with a reducing normalized peak-to-peak change in lift and increasing phase angle as α increases. PIV measurements were taken for an angle of attack, $\alpha = 0°$. The PIV measurements indicated a separated region formed behind the mini-tab, which deflected the streamlines upwards. As the deployment reduced frequency increases, the size and shape of the separation region changes, with the phase angle observable through comparison to the steady-state results.

Acknowledgments

The authors would like to thank Airbus UK for the financial support supplied to this project. The first author's work was supported by a University Research Studentship supplied by the University of Bath. The project was also supported by the University of Bath Alumni Fund and EPSRC grant EP/M022307/1.

References

[1]Federal Aviation Regulations, "Part 25 – Airworthiness Standards: Transport Category Airplanes" *U.S. Department of Transportation, Federal Aviation Administration,* Sept. 1980.

[2]Andersen, P. B., "Advanced Load Alleviation for Wind Turbines Using Adaptive Trailing Edge Flaps: Sensoring and Control.", *Ph.D. Thesis*, Technical University of Denmark, 2010.

[3]Heinz, J., Sorensen, N.N., and Zahle, F. "Investigation of the load reduction potential of two trailing edge flap controls using CFD", *Wind Energy*, Vol 14, 2011, pp.449-462

[4]Kral, L.D., "Active flow control technology", *ASME Fluids Engineering Division Newsletter*, 1999: pp. 3-6.

[5]Heathcote, D.J., Gursul, I., and Cleaver, D.J., "An Experimental Study of Mini-Tabs for Aerodynamic Load Control", 54th AIAA Aerospace Sciences Meeting, AIAA-2016-0325, AIAA, San Diego, 2016.

[6]Al-Battal, N., Cleaver, D.J., Gursul, I., "Aerodynamic Load Control through Blowing", 54th AIAA Aerospace Sciences Meeting, AIAA-2016-1820, AIAA, San Diego, 2016

[7]Liebeck, R.H., "Design of Subsonic Airfoils for High Lift", *Journal of Aircraft*, Vol. 15, No. 9, 1978, pp. 547-561.

[8]Liu, T. and Montefort, J., "Thin-Airfoil Theoretical Interpretation for Gurney Flap Lift Enhancement", *Journal of Aircraft*, Vol. 44, No. 2, 2007, pp. 667-671.

[9]Palacios J., Kinzel, M. K., Overmeyer, A., and Szefi, J., "Active Gurney Flaps: Their Application in a Rotor Blade Centrifugal Field", *Journal of Aircraft*, Vol. 51, No. 2, 2014, pp. 473-489.

[10]Matalanis, C. G., Wake, B. E., Opoku, D., Min, B-Y., Yeshala, N. and Sankar, L., "Aerodynamic Evaluation of Miniature Trailing-Edge Effectors for Active Rotor Control", *Journal of Aircraft*, Vol. 48, No. 3, 2011, pp. 995-1004.

[11]Tang, D and Dowell, E.H., "Aerodynamic Loading for an Airfoil with an Oscillating Gurney Flap", *Journal of Aircraft*, Vol. 44, No. 4, 2007, pp. 1245 - 1257

[12]Kinzel, M.K., Maughmer, M.D., Duque, E.P.N., "Numerical Investigation on the Aerodynamics of Oscillating Airfoils with Deployable Gurney Flaps", AIAA Journal, Vol. 48, No. 7, 2010, pp. 1457-1469.

[13]Theodorsen, T., "General Theory of Aerodynamic Instability and the Mechanism of Flutter," NACA Report. No. 496, 1935.

[14]Lee, H-T and Kroo, I.M., "Computational Investigation of Airfoils with Miniature Trailing Edge Control Surfaces", 42nd AIAA Aerospace Sciences Meeting and Exhibit, AIAA-2004-1051, AIAA, 2004.

[15]Barlow, J. B., Rae, J. B., and Pope. A., *Low-speed wind tunnel testing*, John Wiley & Sons., 1999, pp. 309.

[16]Pankhurst, R. C. and Holder, D. W., *Wind Tunnel Technique: An Account of Experimental Methods in Low- and High- Speed Wind Tunnels*, 1st Edition, Pitman, London, pp. 462- 465.

[17]Wang, J., Li, Y. and Choi, K.-S., "Gurney flap—Lift enhancement, mechanisms and applications*"*, *Progress in Aerospace Sciences*, Vol. 44, No. 1, 2008, pp. 22-47.

[18]Tsai. K-C., Pan T-C., Cooperman, A.M., Johnson, S.J., van Dam, C.P., "An Innovative Design of a Microtab Deployment Mechanism for Active Aerodynamic Load Control", *Energies*,Vol. 8, 2015, pp. 5885-5896.

[19]Kumme, R., "Investigation of the Comparison Method of the Dynamic Calibration of Force Transducers", *Measurement*, Vol. 23, No. 4, 1998, pp. 239-245.

[20]Moffat, R.J., "Using Uncertainty Analysis in the Planning of an Experiment," *Journal of Fluids Engineering-Transactions of the ASME*, Vol. 107, No. 2, 1985, pp. 173-178.

[21]Myose, R., Papadakis, M. and Heron, I., "Gurney Flap Experiments on Airfoils, Wings, and Reflection Plane Model" *Journal of Aircraft*, Vol. 35, 1998, pp. 206-211.

[22]Van Dam, C.P., Yen, D.T., and Vijgen, P.M. H. W., "Gurney Flap Experiments on Airfoil and Wings". *Journal of Aircraft*, Vol. 36, No. 2, pp. 484-486.

Figures

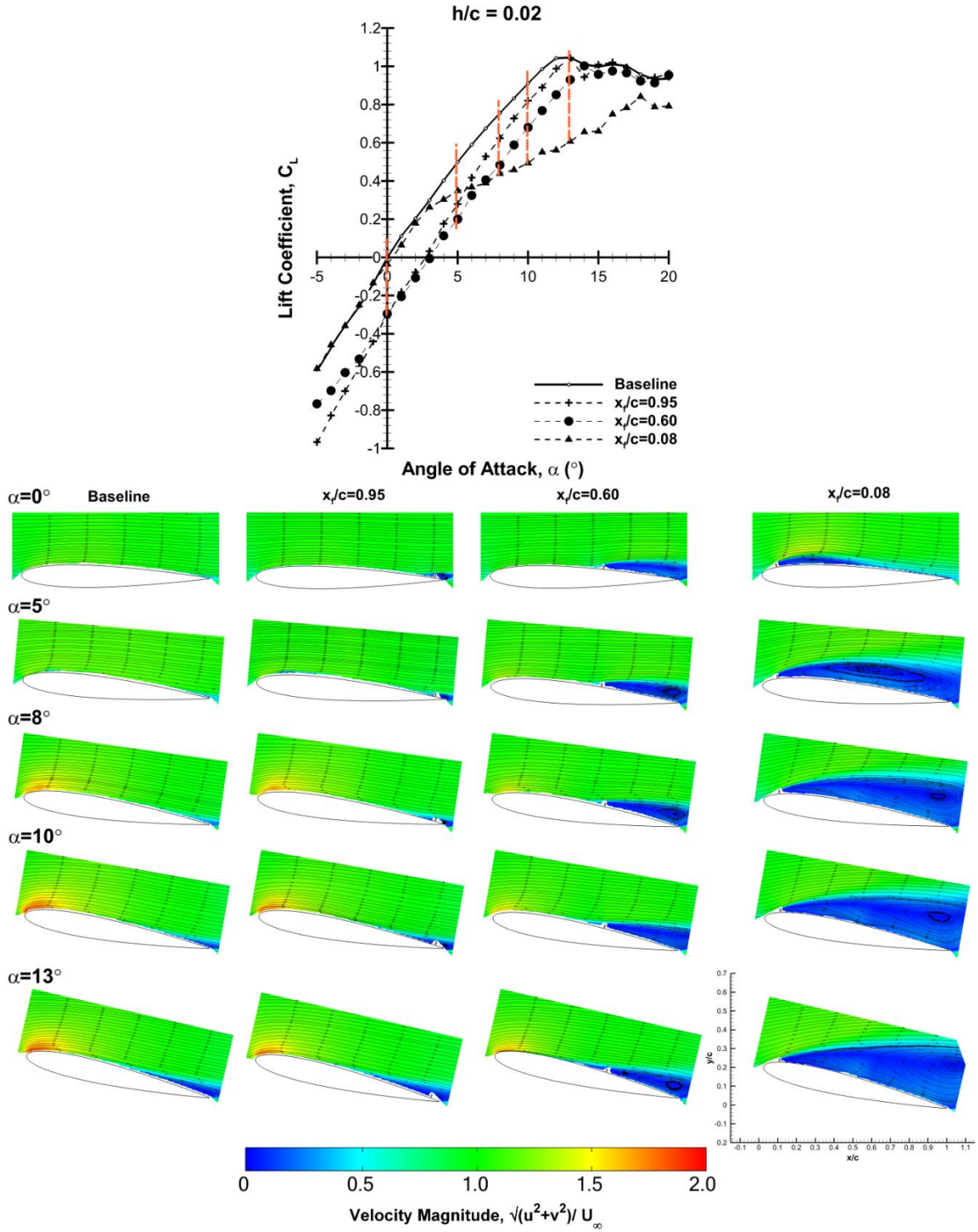

Figure 1: Results from Heathcote et al[5], indicative of a static mini-tab of height, h/c = 0.02. Lift coefficient vs. angle of attack shown from chord-wise positions of x_f/c = 0.08, 0.60 and 0.95. Flow characteristics for corresponding locations are shown as normalized velocity magnitude plots at angles of attack indicated by red vertical lines in the lift coefficient plot.

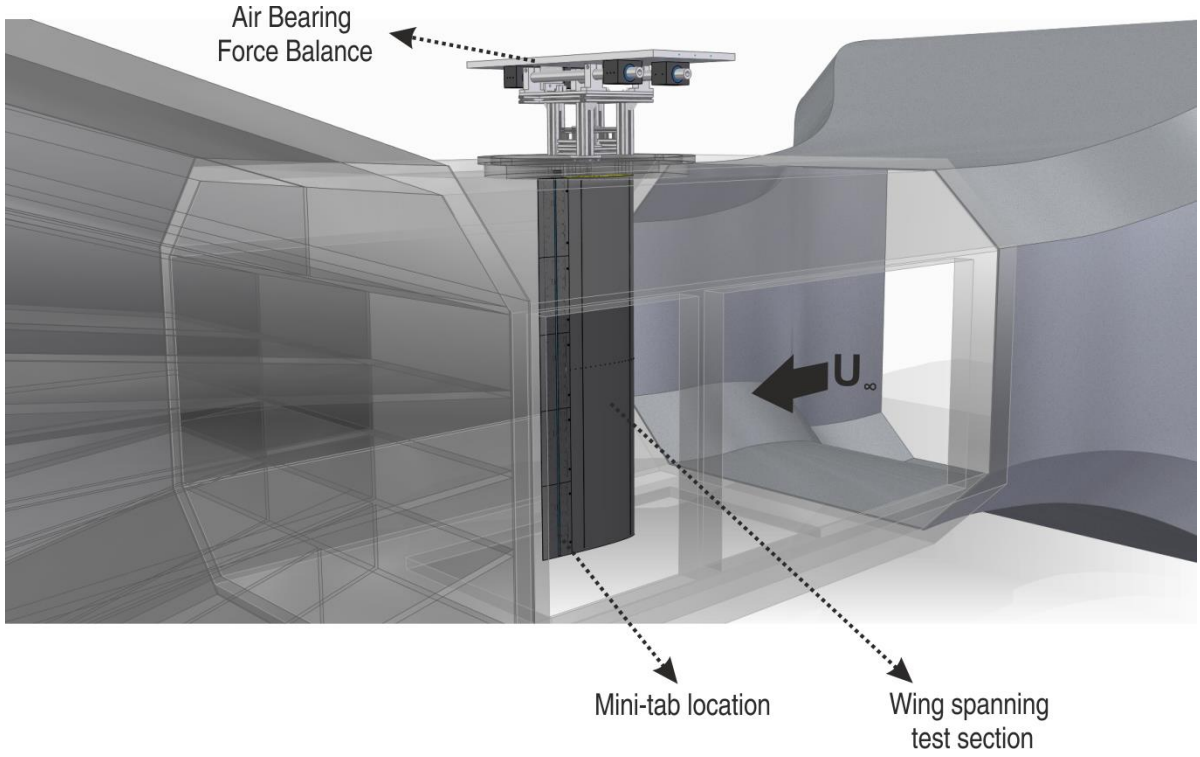

Figure 2: Illustration of the experimental set up used for dynamic mini-tab experiments.

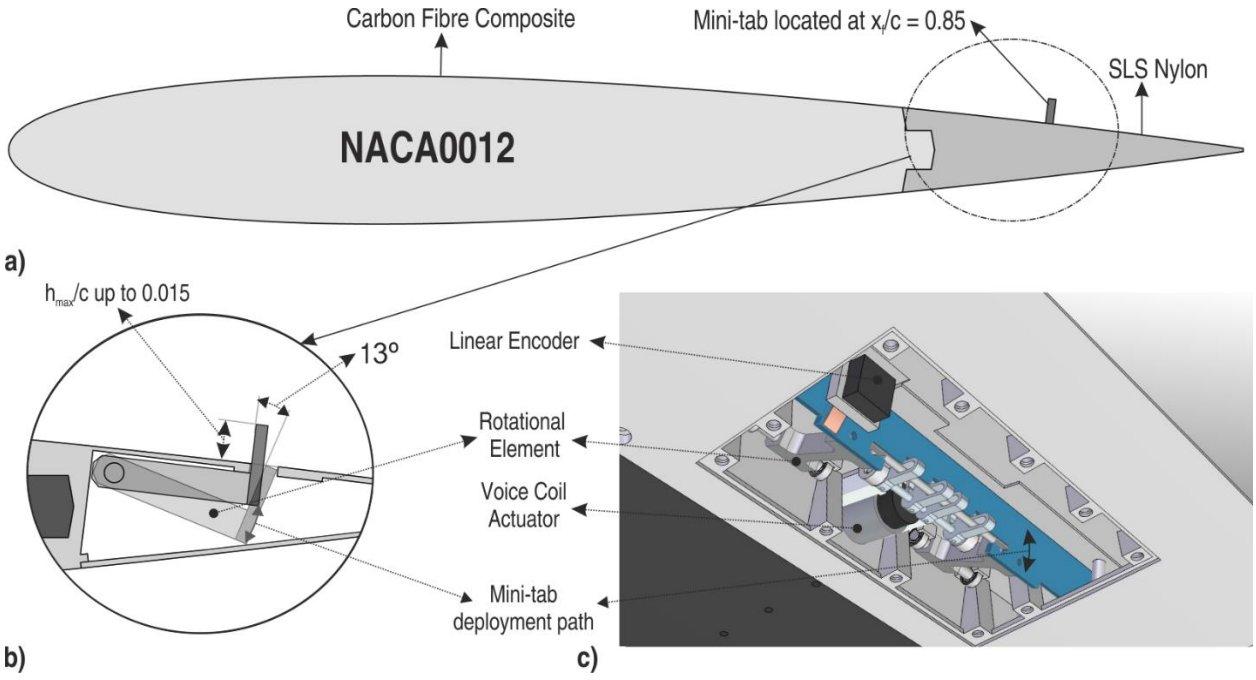

Figure 3: (a) Schematic of NACA0012 profile including mini-tab location, (b) illustration of mini-tab deployment motion (c) illustration of interior of a trailing edge section.

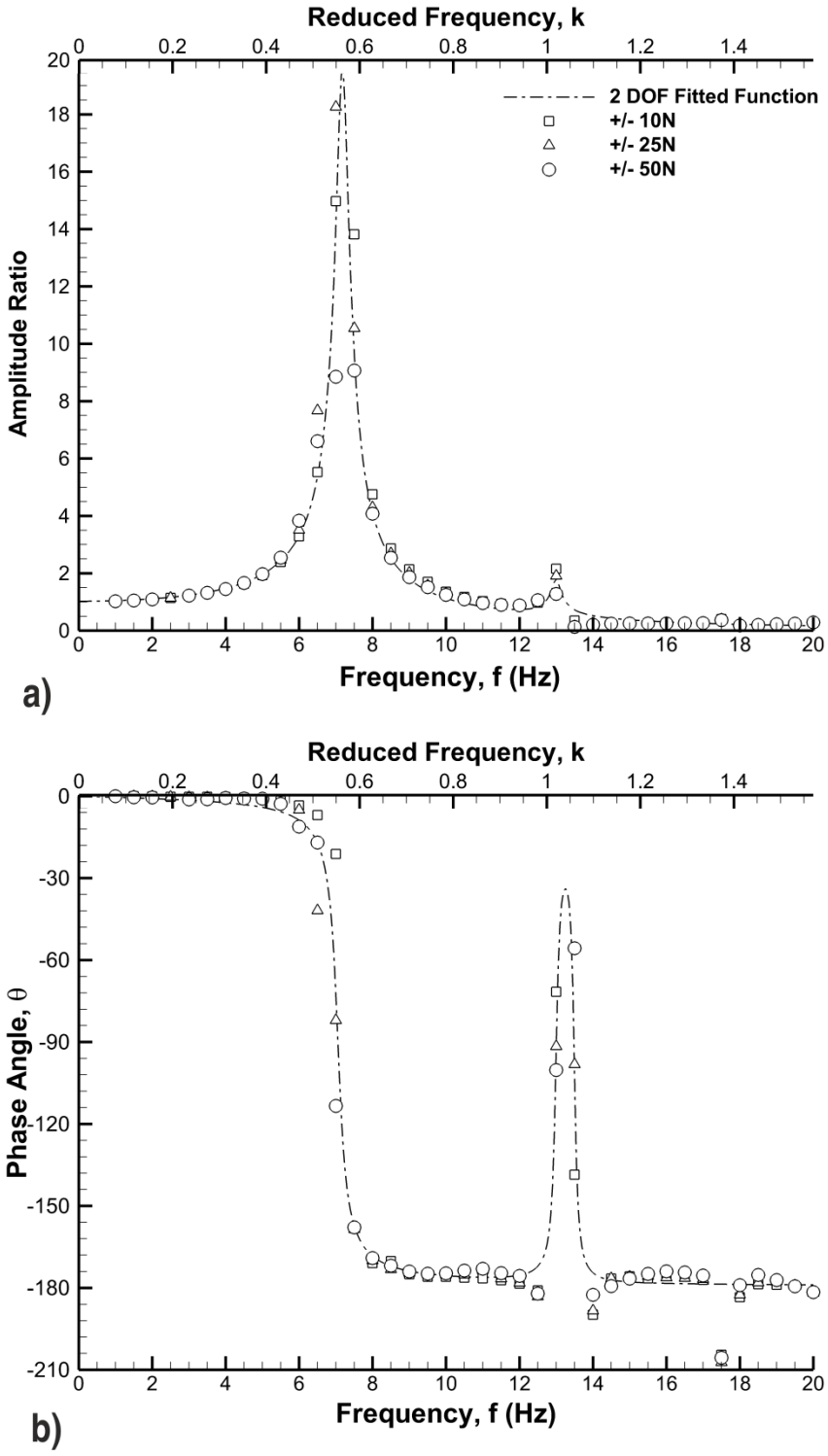

Figure 4: Dynamic force balance calibration, indicating the transfer function between input and measured force in terms of (a) amplitude ratio and (b) phase angle.

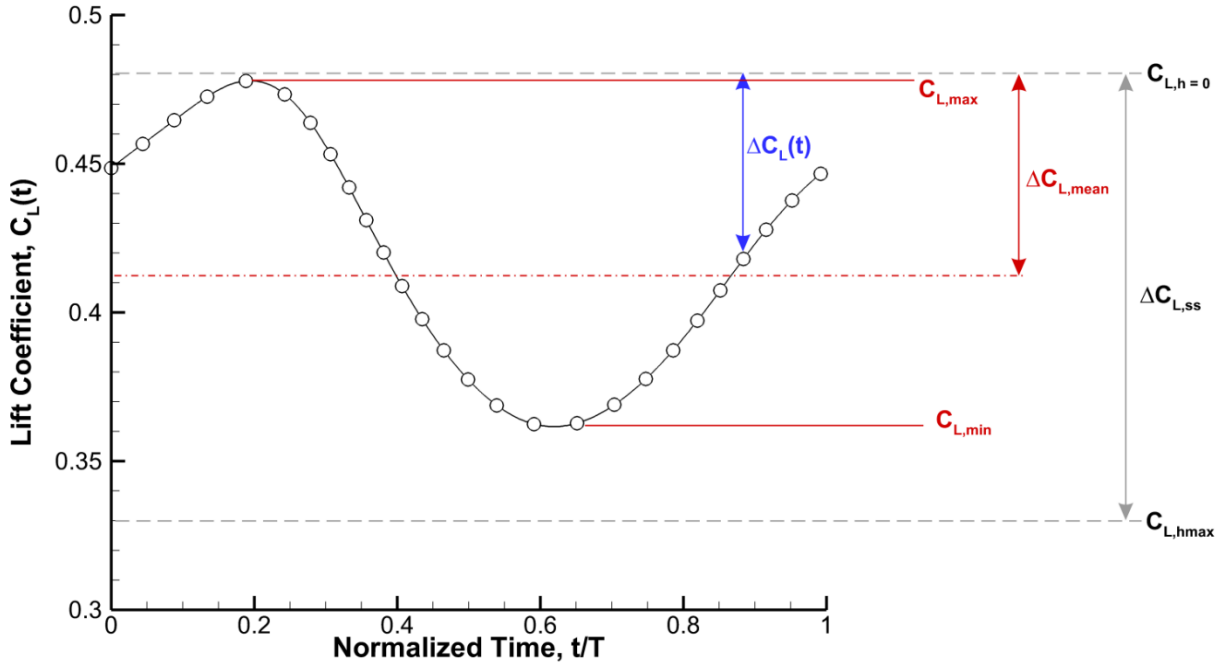

Figure 5: Description of nomenclature used when discussing phase-averaged lift coefficient.

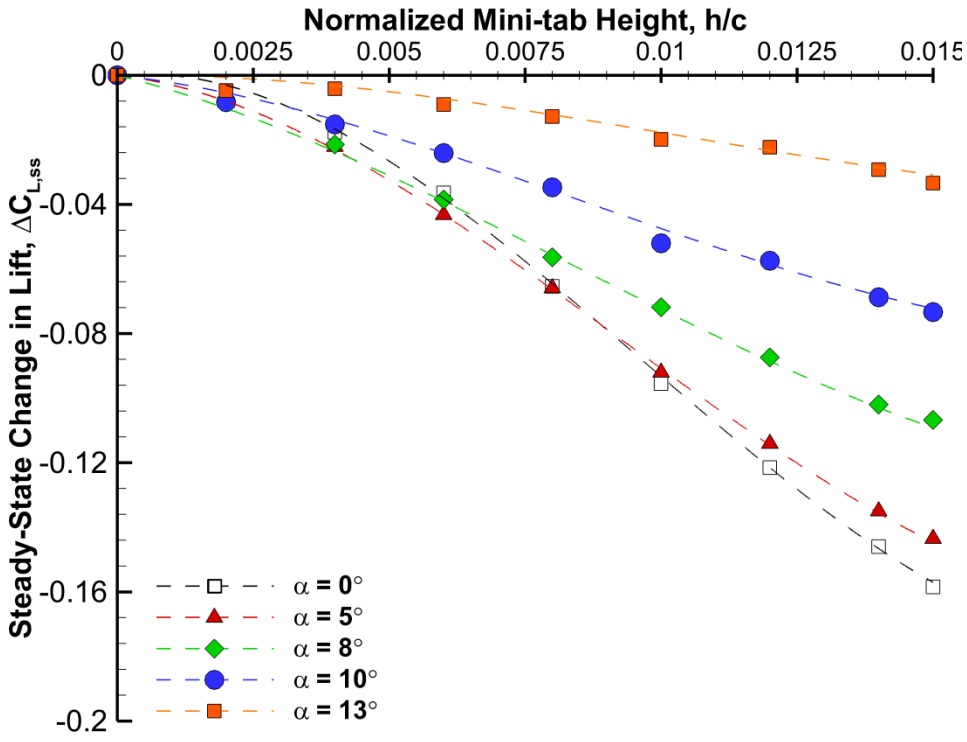

Figure 6: Static change in lift coefficient, $\Delta C_{L,ss}$ vs. normalized mini-tab height, h/c at α = 0 to 13°. Line of best fit for each angle of attack is provided through a cubic polynomial fit.

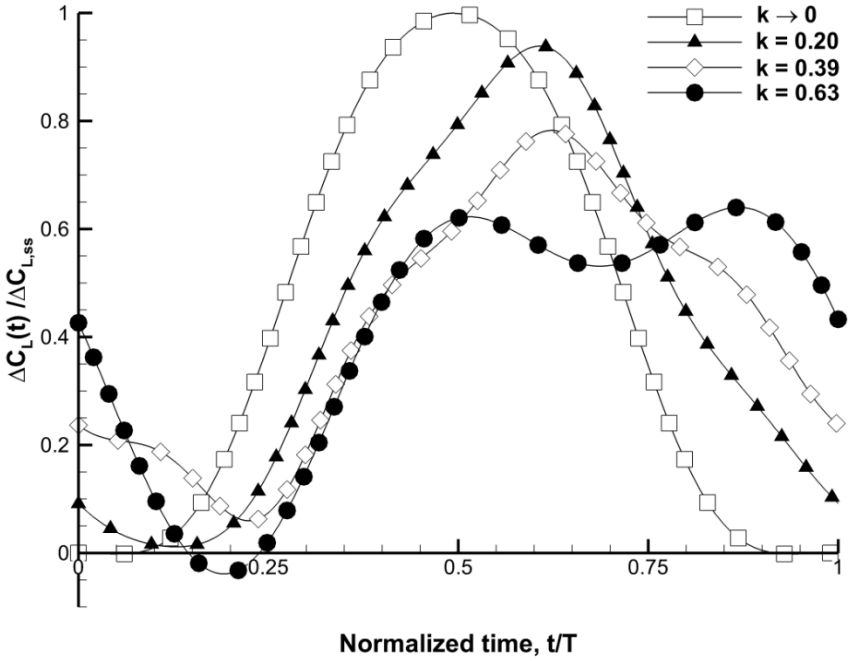

Figure 7: Phase-averaged normalized change in lift, $\Delta C_L(t)/\Delta C_{L,ss}$ for steady state ($k \rightarrow 0$), k = 0.20, 0.39 and k = 0.63 vs. Normalized time, t/T for $\alpha = 0°$

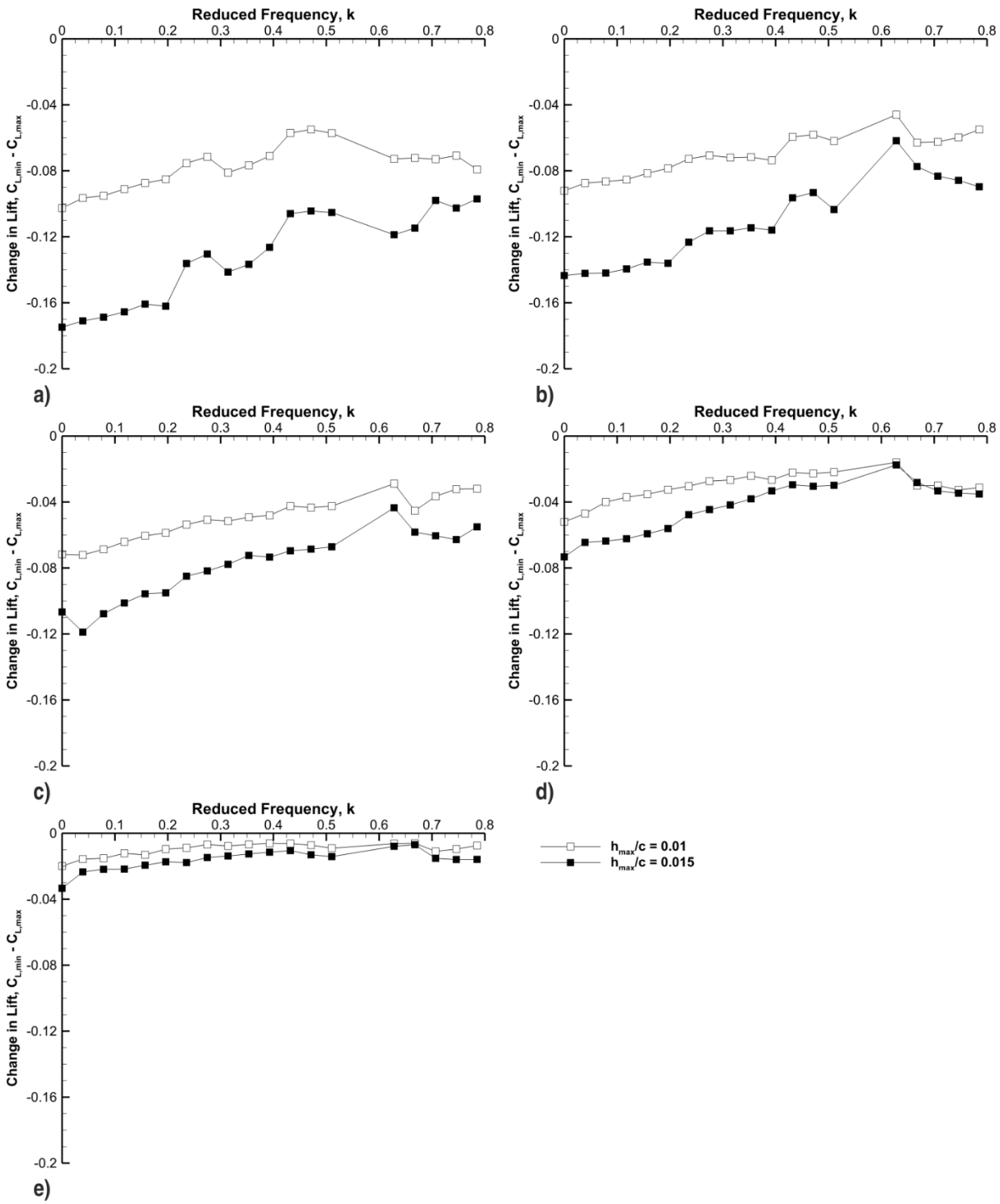

Figure 8: Phase-averaged change in lift, $C_{L,\,min}$ - $C_{L,\,max}$ vs. reduced frequency, k for periodic mini-tab deployments of h_{max}/c = 0.01 and 0.015 at α = (a) 0°, (b) 5°, (c) 8°, (d) 10° and (e) 13°.

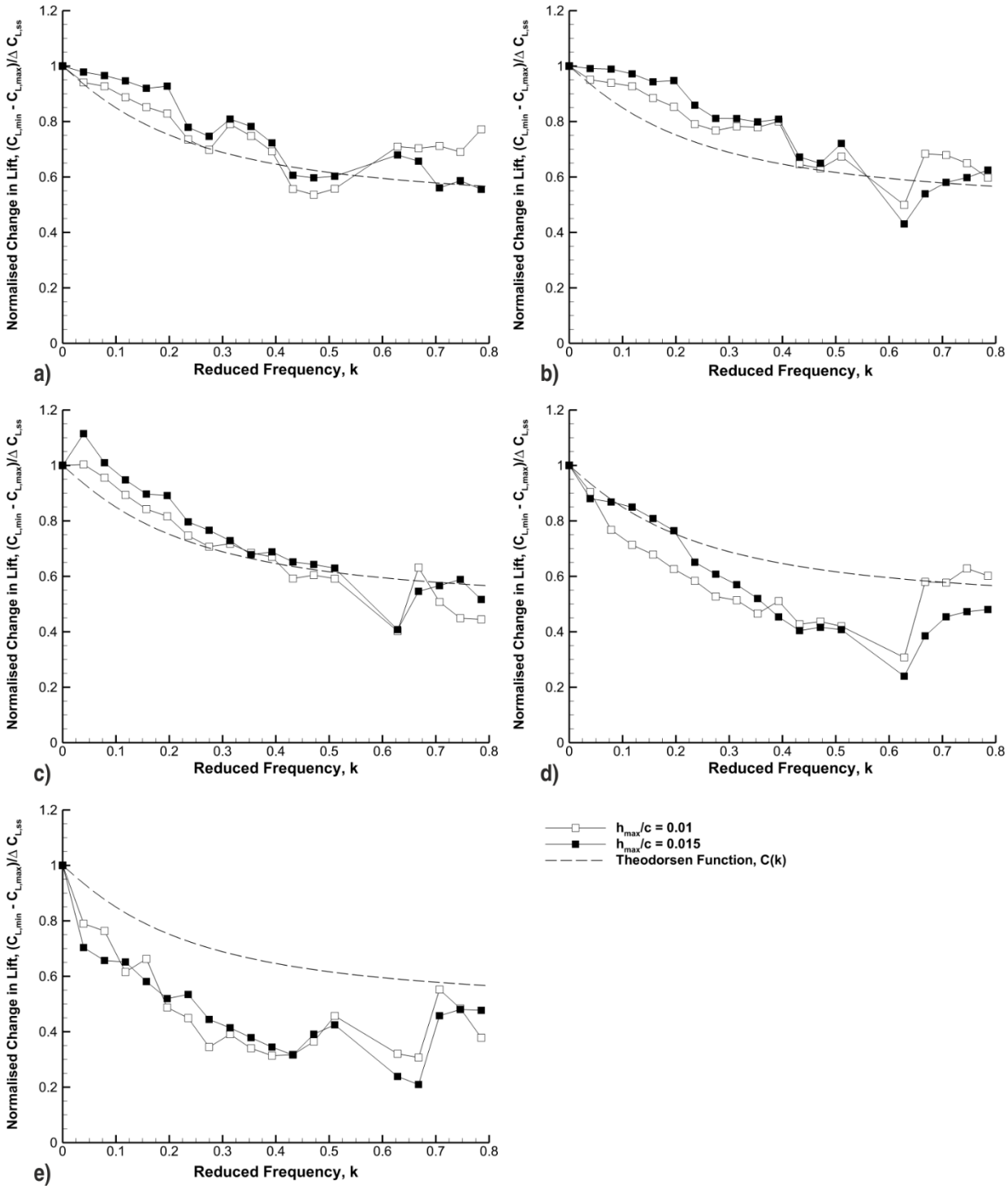

Figure 9: Phase-averaged normalized change in lift, $(C_{L,\ min} - C_{L,\ max})/\Delta C_{L,ss}$ vs. reduced frequency, k for periodic mini-tab deployments of h_{max}/c = 0.01 and 0.015 at α = (a) 0°, (b) 5°, (c) 8°, (d) 10° and (e) 13°.

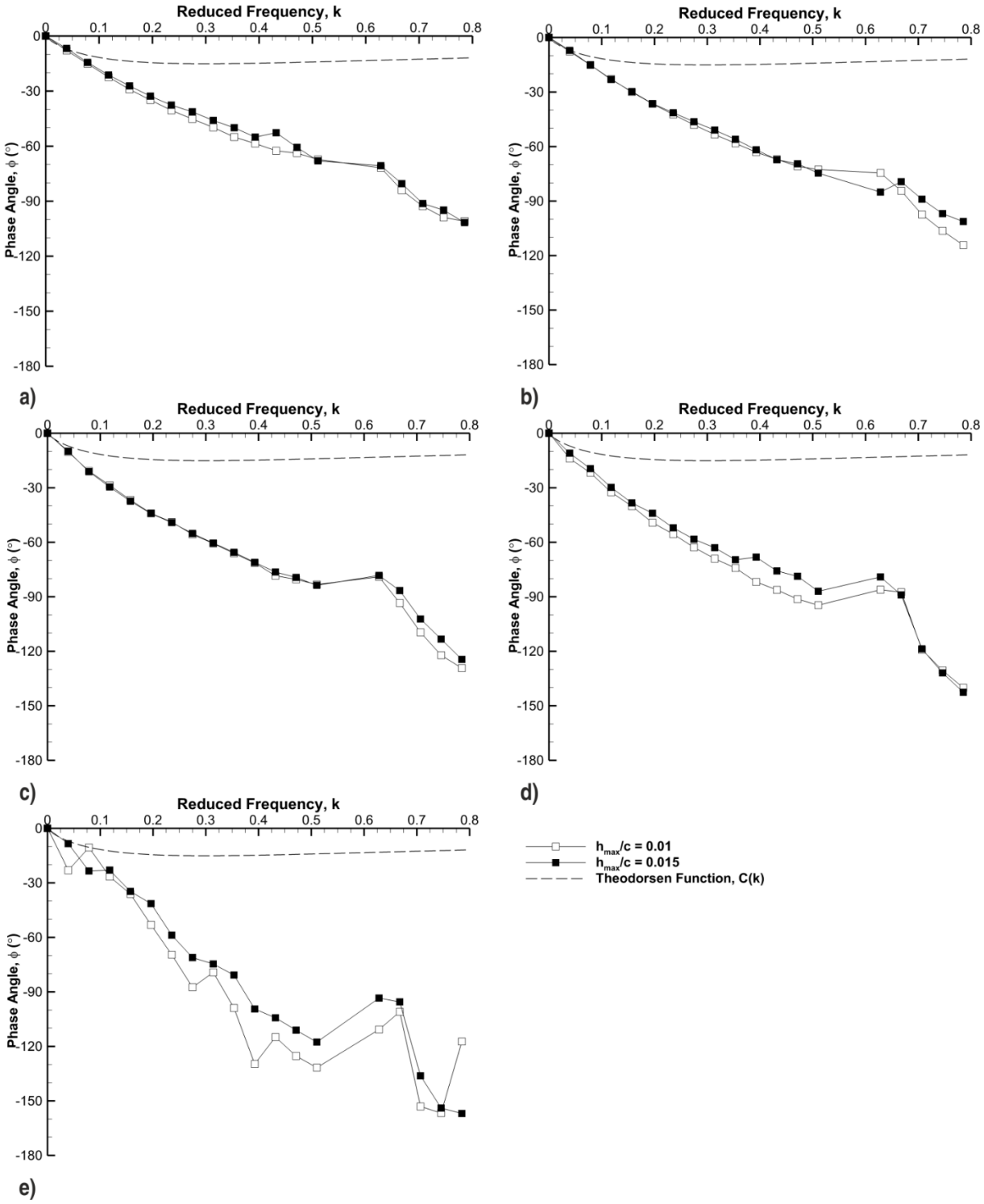

Figure 10: Phase-averaged phase angle, φ vs. reduced frequency, k for periodic mini-tab deployments of h_{max}/c = 0.01 and 0.015 at α = (a) 0°, (b) 5°, (c) 8°, (d) 10° and (e) 13°.

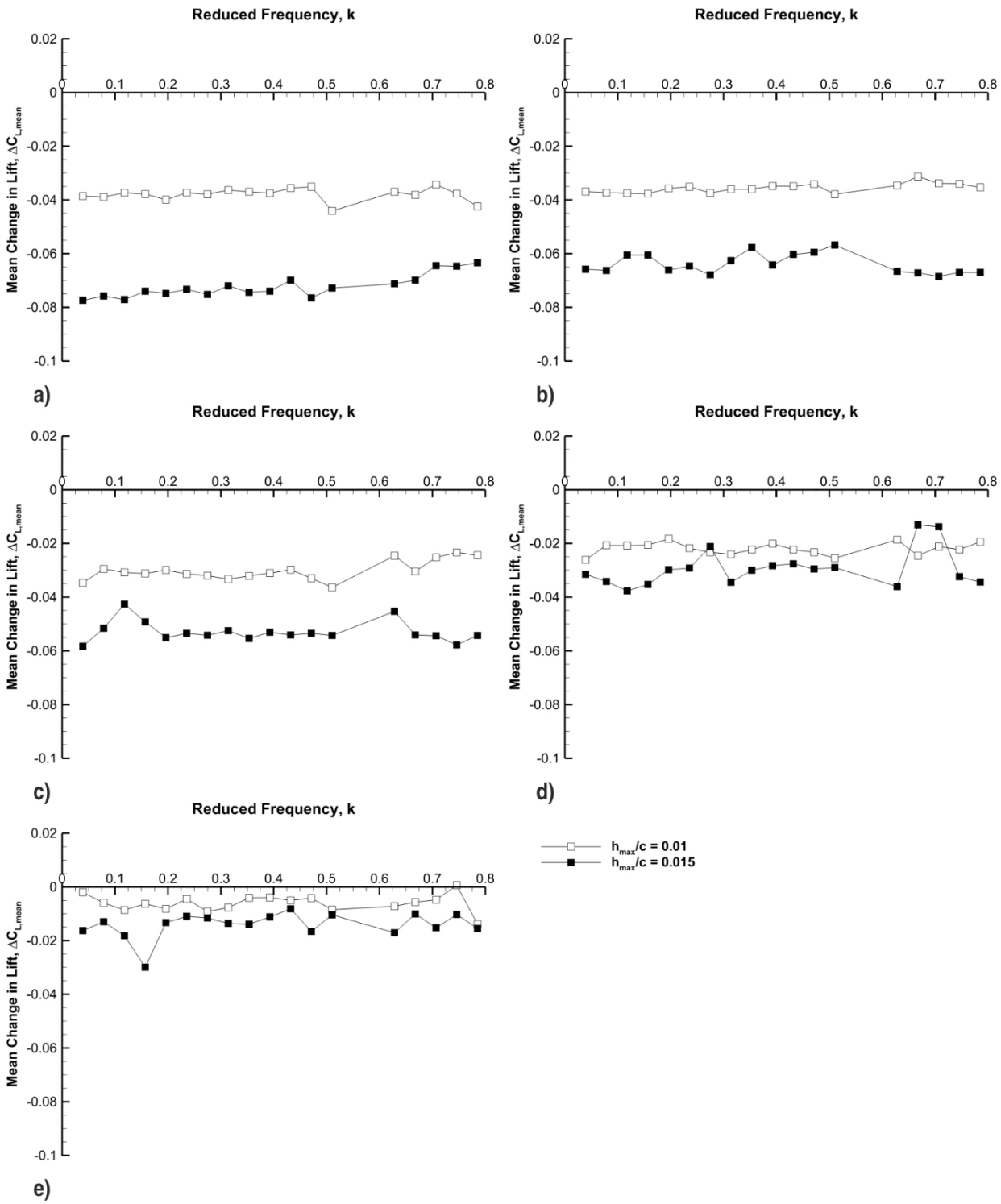

Figure 11: Phase-averaged mean change in lift, $\Delta C_{L,\,mean}$ vs. reduced frequency, k for periodic mini-tab deployments of h_{max}/c = 0.01 and 0.015 at α = (a) 0°, (b) 5°, (c) 8°, (d) 10° and (e) 13°.

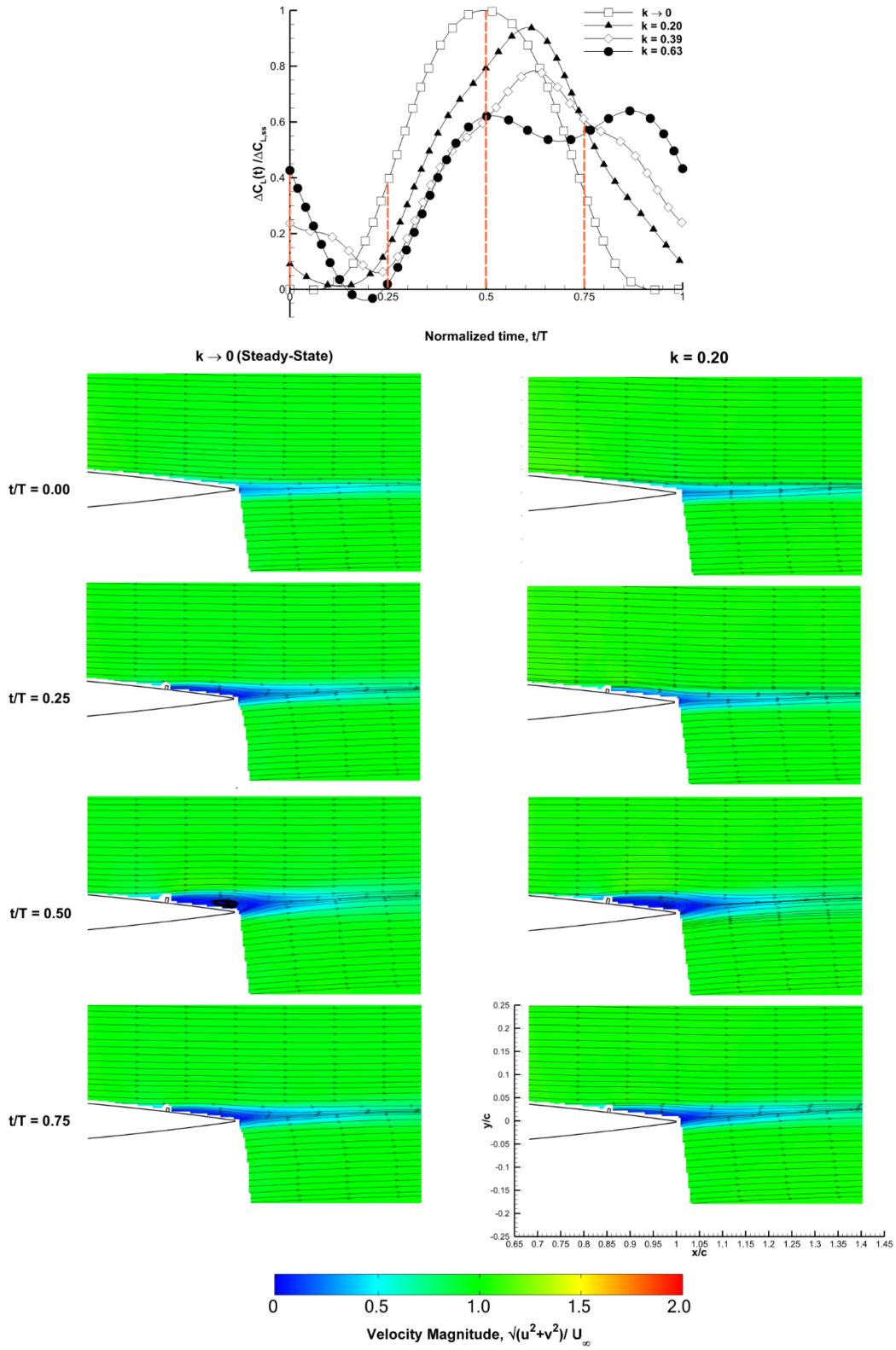

Figure 12: Phase-Locked Particle Image Velocimetry showing velocity magnitude for k → 0 (1st Column), k = 0.20 (2nd Column) at normalized deployment positions of t/T = 0.0, 0.25, 0.5, 0.75 for α = 0°

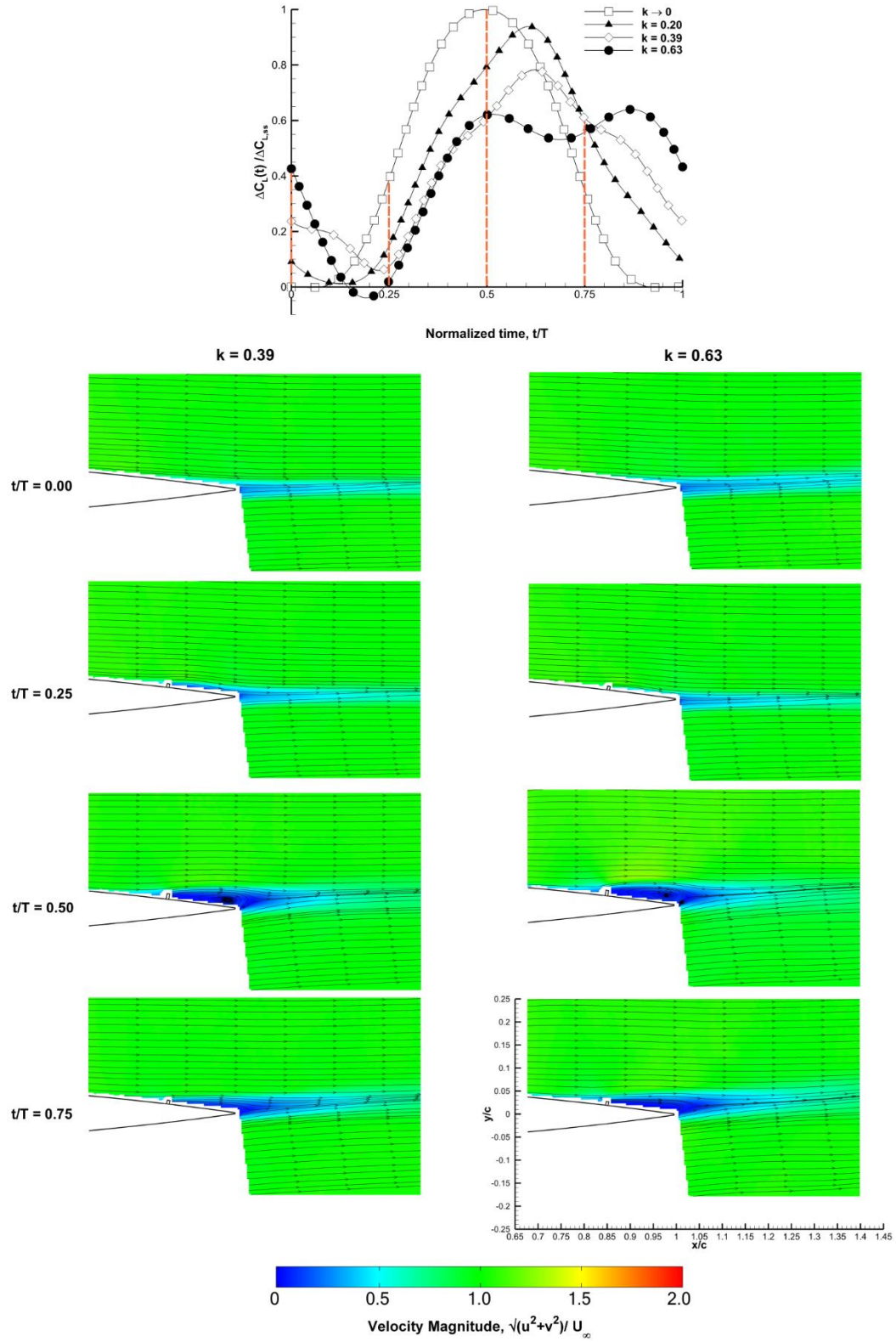

Figure 12 continued: Phase-Locked Particle Image Velocimetry showing velocity magnitude for k = 0.39 (1st Column), k = 0.63 (2nd Column) at normalized deployment positions of t/T = 0.0, 0.25, 0.5, 0.75 for α = 0°

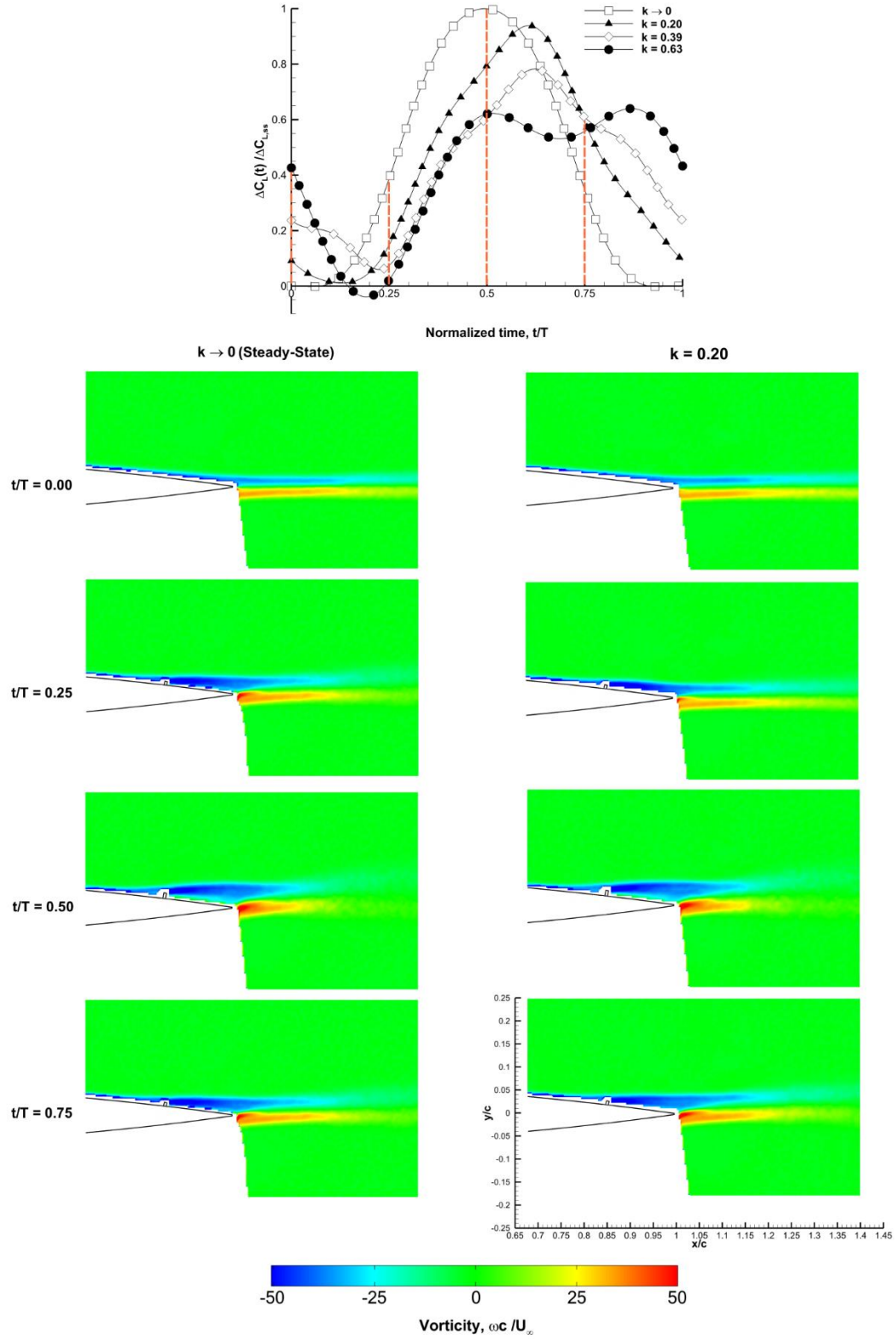

Figure 13: Phase-Locked Particle Image Velocimetry showing vorticity for k → 0 (1st Column), k = 0.20 (2nd Column) at normalized deployment positions of t/T = 0.0, 0.25, 0.5, 0.75 for α = 0°

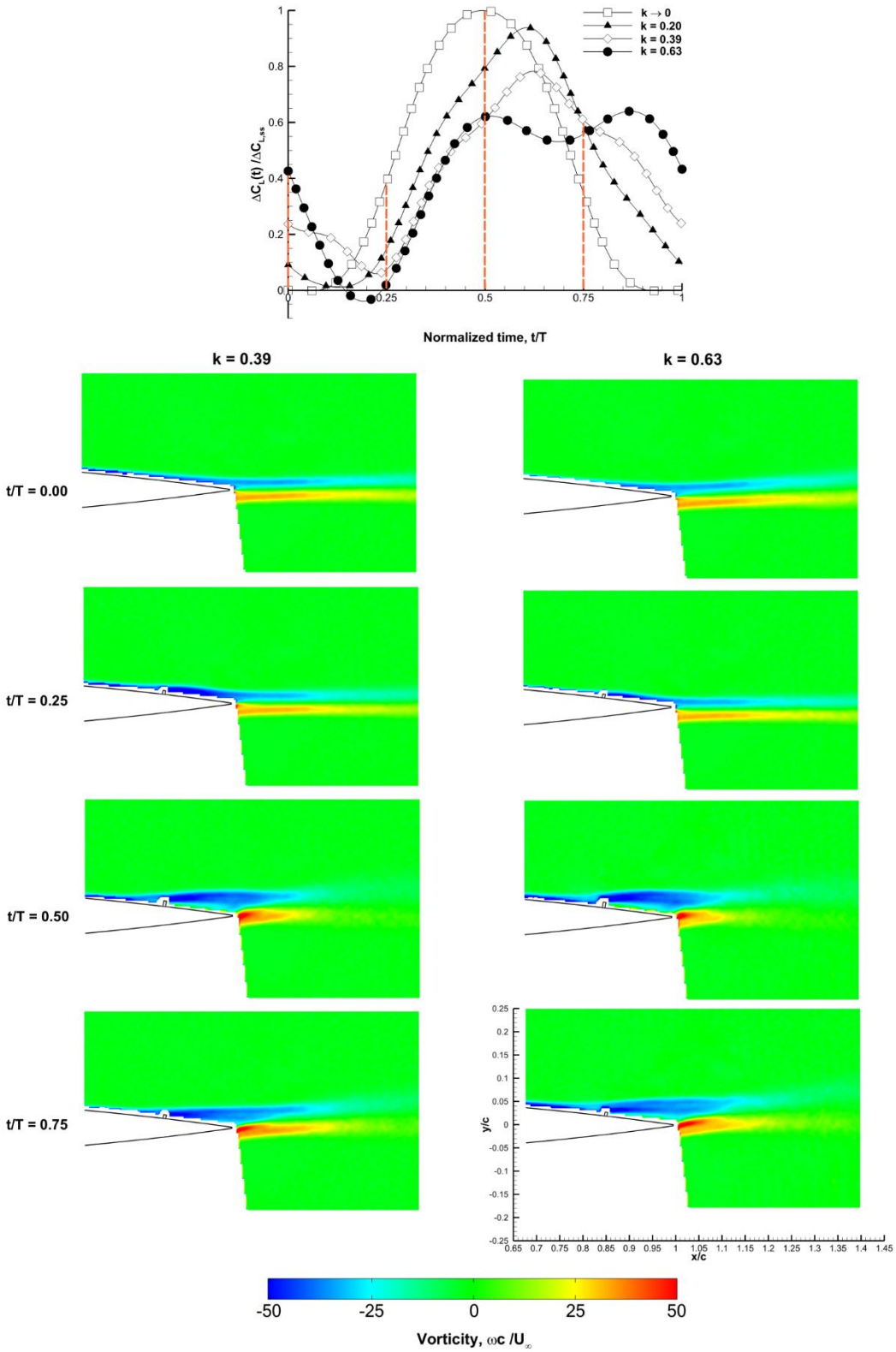

Figure 13 continued: Phase-Locked Particle Image Velocimetry showing vorticity for k = 0.39 (1st Column), k = 0.63 (2nd Column) at normalized deployment positions of t/T = 0.0, 0.25, 0.5, 0.75 for α = 0°